Magnetic microposts for mechanical stimulation of biological cells: Fabrication, characterization, and analysis

Nathan J. Sniadecki,[1] Corinne M. Lamb,[3] Yaohua Liu,[3] Christopher S. Chen,[2] and Daniel H. Reich[3,a)]
[1]*Department of Mechanical Engineering, University of Washington, Seattle, Washington 98195, USA*
[2]*Department of Bioengineering, University of Pennsylvania, Philadelphia, Pennsylvania 19104, USA*
[3]*Department of Physics and Astronomy, Johns Hopkins University, Baltimore, Maryland 21218, USA*

(Received 5 February 2008; accepted 16 March 2008; published online 16 April 2008)

Cells use force as a mechanical signal to sense and respond to their microenvironment. Understanding how mechanical forces affect living cells requires the development of tool sets that can apply nanoscale forces and also measure cellular traction forces. However, there has been a lack of techniques that integrate actuation and sensing components to study force as a mechanical signal. Here, we describe a system that uses an array of elastomeric microposts to apply external forces to cells through cobalt nanowires embedded inside the microposts. We first biochemically treat the posts' surfaces to restrict cell adhesion to the posts' tips. Then by applying a uniform magnetic field ($B<0.3$ T), we induce magnetic torque on the nanowires that is transmitted to a cell's adhesion site as an external force. We have achieved external forces of up to 45 nN, which is in the upper range of current nanoscale force-probing techniques. Nonmagnetic microposts, similarly prepared but without nanowires, surround the magnetic microposts and are used to measure the traction forces and changes in cell mechanics. We record the magnitude and direction of the external force and the traction forces by optically measuring the deflection of the microposts, which linearly deflect as cantilever springs. With this approach, we can measure traction forces before and after force stimulation in order to monitor cellular response to forces. We present the fabrication methods, magnetic force characterization, and image analysis techniques used to achieve the measurements. © *2008 American Institute of Physics.*
[DOI: 10.1063/1.2906228]

I. INTRODUCTION

Biological cells sense and respond to mechanical forces arising in their local environment, which can lead to physiologic or pathologic changes in cell and tissue function.[1] Cells detect mechanical force through a class of unique subcellular structures. Chief among these are focal adhesions (FAs), which are complexes that anchor cells to the surrounding extracellular matrix (ECM).[2] FAs respond to mechanical force by initiating biochemical signals that lead to changes in cellular function and cytoskeletal structure, a process known as mechanotransduction.[3] Thus, techniques that can apply local forces to cells can provide insight into how mechanotransduction at FAs drives cell function. Optical tweezers,[4–6] magnetic beads,[7–9] microneedles,[10,11] and atomic force microscopy[12] have been used to apply 10 pN–100 nN forces to cells to mimic the forces encountered *in vivo* and to measure the local response to such forces.[13] These techniques have demonstrated that cells adjust both their adhesive strength and biochemical signaling levels at the local site of force application,[14,15] but it is unclear whether such forces affect the global contractile state of the cell, which also plays a role in mechanotransduction and cellular function.[16–19]

Previous force-stimulation techniques lack the means to measure a cell's traction forces, which it uses to migrate, contract, divide, or adjust cytoskeletal tension and thereby send mechanical signals to its FAs. Measuring traction forces is possible through plating cells onto flexible substrates and recording the distortions caused by those forces (1–100 nN) on the substrate.[20,21] Approaches to this method include using flat, soft materials that deform[22–25] or arrays of microfabricated microposts that bend under traction forces.[26,27] Combining the abilities to apply forces to FAs and to measure traction forces would enable a more complete understanding of how forces outside and inside a cell affect its mechanotransduction response.

Here, we report the design, characterization, and implementation of a new biological tool that can stimulate the adherent surface of single cells and simultaneously measure their traction forces in a spatiotemporal fashion. Our technique, based on micro- and nanofabrication methods, involves the culturing of cells on the top surface of an array of flexible, polydimethylsiloxane (PDMS) microposts [Fig. 1(a)]. We microcontact print ECM protein onto the microposts so that cells spread only on the tips. As a cell contracts or migrates, each micropost deflects in proportion to the local traction force at the adhesion site where the cell contacts it [Fig. 1(b)]. We record the deflections δ with a microscope in order to measure the changes in traction forces over time.

a)Electronic mail: reich@jhu.edu.

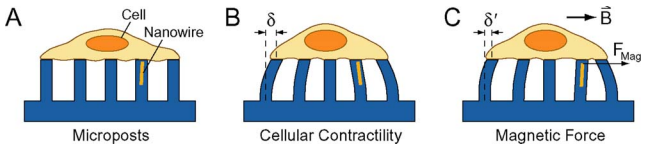

FIG. 1. (Color online) Illustration of the magnetic micropost array. (A) Cells are plated onto the micropost arrays that contain embedded cobalt nanowires. Microposts have 3 μm diameters, 10 μm heights, and 9 μm center-to-center spacing. Nanowires have 350 nm diameters and are 5–7 μm in length. (B) Traction forces from the cell impart deflections δ to the microposts. These deflections are measured to calculate the local traction force. (C) Application of a uniform magnetic field **B** induces a magnetic torque on the nanowire that causes an external force F_{mag} on the cell. Force stimulation causes a change in traction forces δ' that can be readily detected.

Unlike other force measurement techniques, the microposts are mechanically isolated from each other and thereby provide independent spatially resolved readout of the traction forces. To apply forces to cells, we embed magnetic nanowires into a subset of the microposts. A uniform, horizontally applied magnetic field creates a torque on the nanowires, which transfers an external force to cells adherent on these "magnetic" microposts [Fig. 1(c)]. We monitor changes in the traction forces before and after applying the field and can apply forces to cells with negligible interference to the traction force measurement readings. Moreover, we can apply forces and probe the response at mature basal FAs, which has not been examined before by other force-stimulation techniques. This technique takes advantage of the high magnetic moment and anisotropic properties of the nanowires to enable the application of external loads to cells as large as 45 nN. In the first set of experiments with this system, we observed that application of external forces led to losses in traction forces, showing that cells mechanically adapt to forces in their environment.[28] In this paper, we describe the fabrication, operation, and capabilities of the magnetic micropost system.

II. MECHANICS OF MICROPOST DEFLECTION

The microposts that we use in our system have height $L=10$ μm and diameter $d=3$ μm. We have previously studied the mechanical properties of nonmagnetic microposts (i.e., posts that do not contain magnetic nanowires)[26,29] and have found that for forces $F<100$ nN applied at their tips, the deflection δ of the post tips is linear in F. The posts can be adequately modeled by regarding them as one-dimensional cantilevers that bend by an amount

$$\delta = \frac{64L^3}{3\pi E d^4} F, \tag{1}$$

where E is the modulus of elasticity of PDMS (Refs. 26 and 30) [Fig. 1(b)]. We have measured the curvature of deflected microposts and studied the force-deflection relationship with finite element modeling and have found that Eq. (1) is well suited for reporting the local traction forces.[29] For our nonmagnetic microposts, the spring constant $k=3\pi E d^4/64L^3 = 32$ nN/μm.[26]

A cobalt nanowire embedded in a micropost has a magnetic dipole moment $\boldsymbol{\mu}$ predominately oriented along the long axis of the micropost. When subjected to a uniform magnetic field **B**, the nanowire experiences a torque $\tau=\boldsymbol{\mu}\times\mathbf{B}$. Without a cell attached, τ induces a deflection in the magnetic micropost. The δ_M versus τ relationship can be calculated using Castigliano's method[30] by evaluating the strain energy of the micropost-nanowire system under a virtual force P at its tip $(x=L)$. This relationship is given by

$$\delta_M = \frac{\partial}{\partial P}\int_0^L \frac{32M^2(x)}{E\pi d^4} dx, \tag{2}$$

where $M(x)$ is the bending moment in the micropost. We note that $M(x)=P(L-x)-\tau$ for $0\leqslant x<L_w$ and $M(x)=P(x-L)$ for $L_w\leqslant x<L$, where L_W is the nanowire length. The modulus of elasticity is $E=E_{\mathrm{PDMS}}$ for $0\leqslant x<L-L_w$ and $E\approx E_{\mathrm{Co}}$ for $L-L_w\leqslant x<L$. Since $E_{\mathrm{Co}}\gg E_{\mathrm{PDMS}}$, upon evaluating Eq. (2) and setting $P=0$ at $x=L$, the deflection due to the magnetic torque is given by

$$\delta_M = \frac{32\tau}{E_{\mathrm{PDMS}}\pi d^4}(L^2 - L_W^2). \tag{3}$$

When a cell is attached to a magnetic micropost, the magnetic torque transfers to the cell as a local force F_{mag} at its adhesion site. Using Castigliano's method again, but this time with the micropost's tip constrained by its interaction with the cell, we let $P=F_{\mathrm{mag}}$ be the reaction force at the cell and set $\delta_M=0$ at $x=L$. This yields

$$F_{\mathrm{Mag}} = \frac{3\tau(L+L_w)}{2(L^2+L_wL+L_w^2)}. \tag{4}$$

For nanowires with $L_w=5-7$ μm and $B=0.2$ T, we have achieved free-end displacements ranging from 0.1 to 1 μm which indicates that applied forces (F_{mag}) between 1 and 45 nN are possible.

III. MAGNETIC MICROPOST DEVICES

Arrays of microposts are fabricated via replica molding using PDMS molds made from an SU-8 photoresist master. Cobalt nanowires are seeded into the PDMS molds and encapsulated in the final PDMS casting to create the magnetic micropost arrays. The arrays are impregnated with a fluorescent dye to enable visualization of the microposts' deflections, and the surfaces of the arrays are then functionalized to restrict cell adhesion to the tips of the microposts.

A. SU-8 master

Master copies of the micropost arrays are made out of SU-8 photoresist via contact photolithography [Fig. 2(a)].[26,31] First, SU-8 2002 photoresist (MicroChem, Newton, MA) is spin coated at 3000 rpm onto a 3 in. silicon wafer, flood exposed in a contact mask aligner (MJB-3, Karl Suss, Waterbury, VT) with an *i*-line dosage of 70 mJ/cm^2, and postexposure baked at 65 °C for 1 min and 95 °C for 2 min to form the base layer of the micropost array. A second layer of photoresist (SU-8 2010) is spun at 4000 rpm, exposed through a chrome mask (Advanced Reproductions, North Andover, MA) at the same dosage, postexposure baked, and serially developed in propylene glycol methyl ether acetate, isopropanol, and hexane to create the patterned array of micropost structures in SU-8 [Fig. 2(b)]. The arrays

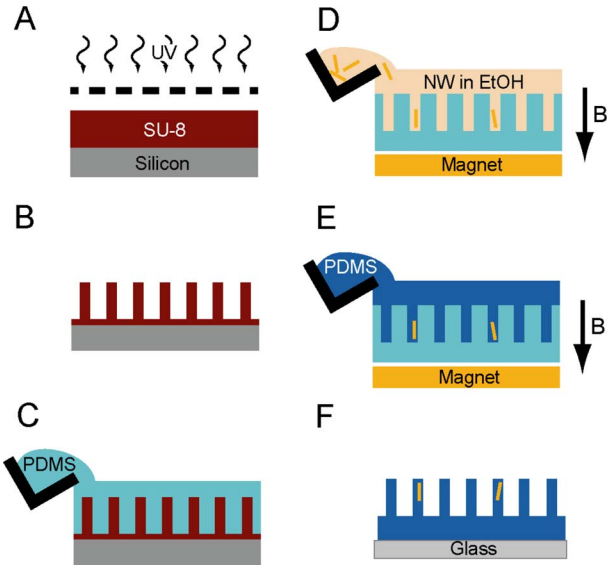

FIG. 2. (Color online) Fabrication of magnetic micropost arrays. (A) SU-8 photoresist is spin coated onto a silicon wafer and exposed with 365 nm light through a photomask to pattern the SU-8. (B) Developing the resist results in freestanding SU-8 microposts. (C) Micropost arrays are cast in PDMS to create negative molds. (D) Nanowires suspended in ethanol are aliquoted into the negative molds while under a magnetic field **B** to draw the nanowires into the holes. (E) PDMS is poured into the template to encapsulate the nanowires. (F) The array is peeled from the template and contains both magnetic microposts with nanowires and nonmagnetic microposts.

we have used for these studies have micropost diameter $d=3$ μm, height $L=10$ μm, and 9 μm center-to-center spacing. The arrays have overall dimensions of 1×1 cm^2 and have a grid of numbers fabricated into them that enable reproducible navigation to desired locations, such as the positions of individual cells or magnetic microposts.

B. Magnetic cobalt nanowires

Cobalt nanowires are grown by electrochemical deposition in the pores of a 50 μm thick porous template with a 350 nm pore diameter (Al_2O_3, Anodisc, Whatman, Inc., Florham Park, NJ). A copper film of 0.5 μm thick sputtered onto the bottom side of the template serves as the working electrode for deposition. The template is placed into a custom-built electrodeposition cell with the top side in contact with a metal solution (0.5*M* $CoSO_4$, 0.5*M* NaCl, 0.8*M* H_3BO_4) at *p*H 3.3. Cobalt nanowires are formed in the pores of the template under an applied voltage of −1.0 V (Ag/AgCl). We control the lengths of the nanowires by monitoring the total deposited charge. To collect the nanowires, the copper film is first etched away in a solution of 0.1*M* $CuCl_2$ and 1*M* HCl, and then the template is dissolved in deoxygenated KOH in two stages: 20 h in a solution with *p*H 12.8 followed by 4 h in a solution at *p*H 12.4. The freed nanowires are precipitated from solution against the side of a flask with a permanent magnet and serially washed in ethanol. The nanowires in ethanol solution are then sonicated for 5 min to redisperse them.

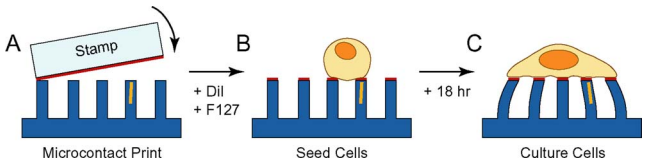

FIG. 3. (Color online) (A) Preparation of the magnetic microposts starts with microcontact printing of fibronectin onto the microposts. A hydrophobic, fluorescent dye (DiI) impregnates the PDMS for fluorescent microscopy. Pluronics F127 NF (F127) is adsorbed to the PDMS to block cellular adhesion from the sidewalls and base. (B) Cells are plated on the microposts and allowed to spread on the fibronectin surface. (C) After culturing overnight (18 h), the cells are ready for testing.

C. Magnetic microposts

Negative molds for casting the PDMS micropost arrays are formed from the SU-8 master and are made from PDMS (Sylgard 184, Dow Corning, Midland, MI) mixed at a 10:1 ratio of base polymer to curing agent that is poured over the SU-8 master and cured at 110 °C for 15 min [Fig. 2(c)]. The molds are then peeled from the master and treated in a plasma etcher (SPI Supplies, West Chester, PA) for 2 min to activate the PDMS surface groups. Next, the molds are placed in a desiccator with 100 μl liquid (tridecafluoro-1,1,2,2-tetrahydrooctyl)-1-trichlorosilane (United Chemical Technologies, Bristol, PA). The desiccator is continuously pumped overnight with the negative molds inside to allow the silane vapor to diffuse over the surface and into the holes as it bonds to the PDMS surface groups. This coating prevents subsequent PDMS castings from sticking to the PDMS molds.[32]

Nanowires with 5–7 μm lengths are suspended in ethanol and aliquotted over the surface of a mold under the presence of a vertical magnetic field from a NdFeB magnet underneath the mold (ForceField, Fort Collins, CO) [Fig. 2(d)]. This field vertically aligns the nanowires and draws them down into the micropost template holes in the mold. After evaporating the ethanol at 70 °C on a hotplate, a 10:1 mixture of PDMS prepolymer is poured over the mold [Fig. 2(e)]. A glass cover slip is placed on the prepolymer, which is then cured at 110 °C for 20 h with a magnet underneath to hold the nanowires in place. When peeled from the molds, the micropost array devices remain fixed to the cover slips [Fig. 2(f)]. During this process, some microposts may collapse or bend to touch their neighbors. These microposts may be freed by sonication in ethanol for 5 min followed by drying with supercritical CO_2 in a critical-point dryer (Tousimis, Rockville, MD).

D. Chemical functionalization

The ECM protein fibronectin is printed onto the tips of the microposts [Fig. 3(a)] to promote cell adhesion. The fibronectin (5 μg/ml, BD Bioscience, San Jose, CA) is adsorbed for 1 h onto a flat PDMS stamp (made with 30:1 ratio of base polymer to curing agent) and then dried with nitrogen. The micropost arrays are treated with UV ozone for 7 min to render the surface hydrophilic for protein transfer and stamped with the fibronectin-coated stamp.[33] The arrays are transferred into ethanol to sterilize them and then fluorescently stained with DiI (1,10-dileyl-3,3,30, 30-

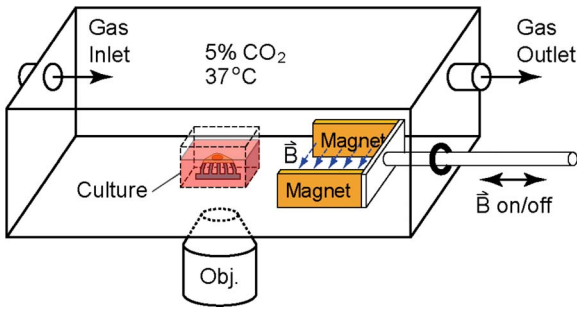

FIG. 4. (Color online) Schematic of the setup for live-cell measurements. Cells on the micropost array are placed in a custom-built microscope chamber that has a sliding rail system with NdFeB magnets to apply a uniform horizontal magnetic field across the array. Temperature and CO_2 levels are controlled to ensure viability of the cells. The arrays are placed inside a glass-bottom cubic culture dish with medium and video recorded on an inverted fluorescence microscope (not drawn to scale).

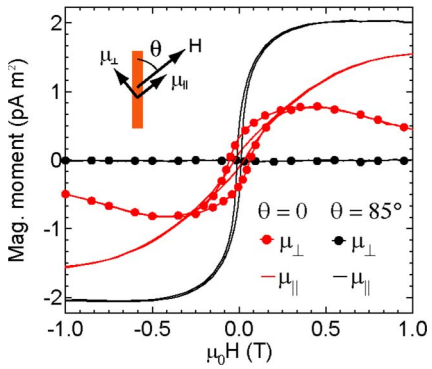

FIG. 5. (Color online) Measurement at room temperature of magnetic moment $\boldsymbol{\mu}$ per cobalt nanowire vs magnetic field $\mu_0 H$ shows different magnetizations for applied field angle θ. Inset: Schematic of H oriented at angle θ to the long axis of the nanowire and magnetic moment components $\mu_\perp$ and $\mu_\parallel$ in the parallel and perpendicular directions.

tetramethylindocarbocyanine methanesulfonate, Invitrogen, Carlsbad, CA) at 5 mg/ml for 1 h. The walls of the microposts and the regions of the arrays between the microposts are then blocked from further protein adsorption by chemical treatment with 0.2% Pluronics F127 (BASF, Ludwigshafen, Germany) for 30 min. This antiadhesive coating restricts cells to adhere only to the tips of the microposts where there is fibronectin during plating and long-term culture [Figs. 3(b) and 3(c)].

E. Magnetic stage incubator

To apply magnetic fields to the micropost arrays during live microscopy measurements, we use a custom-built incubator chamber that fits onto the stage of an inverted microscope (Nikon TE-2000) (Fig. 4). The field is applied with NdFeB magnets (ForceField, Fort Collins, CO), separated by 2.5 cm, on a sliding rail. An array with cells cultured on it is placed at the center of the chamber in a rectangular culture dish ($1.5 \times 1.5 \times 1$ cm^3) with a glass bottom. When the magnets are slid inward, they are positioned at opposite sides of the culture dish to generate a field. In our chamber, the field is 0.2 T at the center of the dish and varies by less than 15% over the area of a micropost array. When the magnets are moved away from the dish, the field on the array is less than 0.005 T. The sliding magnets are also used to apply fields to the array in order to map the locations and measure the deflections of the magnetic microposts before plating cells (Sec. IV E). For the live-cell experiments, the chamber is connected to a temperature and gas controller (LiveCell™; Pathology Devices, Inc., Westminster, MD) to maintain the culture at 37 °C and 5% CO_2.

IV. CHARACTERIZATION OF MAGNETIC MICROPOST ARRAYS

We have characterized the magnetic properties of the cobalt nanowires used in our arrays to find their dipole moments in the directions parallel and perpendicular to an applied field and have verified the encapsulation of the nanowires into the PDMS microposts by optical microscopy and scanning electron microscopy (SEM). We have carried out detailed measurements of the deflection of selected magnetic microposts and have compared the stiffness of the magnetic and nonmagnetic microposts by direct mechanical application of force via pulled-glass microneedles. The position of each magnetic post in an array is recorded prior to the start of live-cell experiments with that array.

A. Magnetic characterization of nanowires

The magnetic properties of the nanowires cannot be accurately measured with the wires in the alumina templates in which they are grown because the close spacing of the pores of the templates yields strong dipole-dipole interactions between the wires.[34,35] Thus, to characterize their magnetic properties, a dilute suspension of nanowires was magnetically oriented under a 0.2 T field, encased in 0.5 mL of epoxy (Araldite 502, Electron Microscopy Science, Hatfield, PA), and measured with a vector vibrating sample magnetometer (DMS model 10, ADE Technologies, Westwood, MA) at room temperature. Figure 5 shows the vector components $\mu_\parallel$ and $\mu_\perp$ of the room temperature magnetic moment $\boldsymbol{\mu}$ per wire for 15 μm long cobalt nanowires measured parallel and perpendicular to the applied field H. Measurements of $\mu_\parallel$ with the field at an angle $\theta=0°$ and $\theta=85°$ to the nanowires' long axis show that $\boldsymbol{\mu}$ preferentially points parallel to the wires' axis due to magnetic shape anisotropy.[36] The remanent magnetic moment $\mu_\parallel(H=0)$ is small due to the presence of magnetocrystalline anisotropy oriented perpendicular to the wires' axis that competes with the shape anisotropy at low field.[37] When H is parallel to the wire ($\theta=0°$), $\mu_\perp$ is approximately zero, but as is shown in Fig. 5, when H is applied nearly perpendicular to the wire's axis ($\theta=85°$), a nonzero $\mu_\perp$ arises for $\mu_0 H < 0.5$ T due to the tendency of $\boldsymbol{\mu}$ to align with the wire. This is important because $\mu_\perp$ determines the magnetic torque τ that generates F_{mag} in our system ($\tau \approx \mu_0 \mu_\perp H$). Note that for the applied field of 0.2 T used to actuate the magnetic microposts in our experiments, the magnitude of $\mu_\perp$ is comparable to or even slightly larger than $\mu_\parallel$. We also note that the magnetic moments of nanowires of 5–30 μm scale simply with their length,[38] and so these results are representative of the 5–7 μm wires we use in the magnetic microposts.

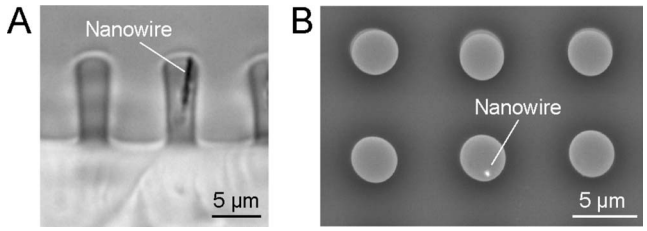

FIG. 6. Microscopy imaging of embedded nanowires in the magnetic microposts. (A) Phase contrast image of a cross-sectioned array showing a nanowire embedded in the microposts. (B) Scanning electron micrograph of the array with the contrast of the cobalt nanowire enhanced with backscattering.

B. Visualization of nanowires in microposts

We confirmed the embedding of the nanowires into the magnetic microposts by cutting cross sections of the arrays with a razorblade and inspecting them via optical microscopy, using a 63× oil immersion objective. Figure 6(a) is a phase contrast image from a side view of an array that shows a nanowire in the upper portion of one of the microposts with $L_w \approx L/2$. Nanowire embedding was also verified by SEM backscattering imaging. In a top view of an array, such as that shown in Fig. 6(b), nanowires appear as bright spots due to the atomic number contrast obtained in this imaging mode between Co and PDMS. We observed that nanowires vary in their orientation from 0° to 15° with respect to the long axis of the micropost; it is this tilt that enables the development of a large $\mu_\perp$ component in a horizontal field.

C. Characterization of magnetic micropost deflections

To measure the displacement of magnetic microposts from the induced torque τ, we applied a uniform horizontal magnetic field **B** using custom-built electromagnets mounted on a Nikon TE-2000 microscope. Magnetic microposts were identified under phase contrast microscopy with a 60× long working distance objective [Fig. 7(a)]. We varied the current in the coils in discrete steps to generate magnetic fields in the range of −0.31 to 0.31 T while imaging the magnetic posts and their nonmagnetic neighbors at each step in the field. An example of a magnetic micropost with a 0.85 μm maximum deflection at **B**=0.31 T is shown in Fig. 7(b). We measured the deflections from the phase contrast micrographs using an image analysis program written in IGORPRO (Wavemetrics, Portland, OR). Each image of the array for a given field strength is thresholded to obtain the centroid of each micropost. The image is brought into registry with the zero-field image (**B**=0) by aligning the centroids of the nonmagnetic posts between images. The deflections of the magnetic microposts are determined from the difference between their zero-field and high-field centroid locations.

We found that applying a 0.31 T field to the array gave displacements δ_M to magnetic microposts in the range of 0.1–1 μm. Figure 7(f) contains measured δ_M versus $\mu_0 H$ curves that show a maximum displacement of 0.37 μm at 0.31 T field for the magnetic micropost shown in Figs. 7(d) and 7(e). The displacement of a given post is always in the same direction, independent of the sign of **B**. This is because, as shown in Fig. 5, $\mu_\perp$ changes sign with **B** and hence the torque always has the same sign. However, the posts do not all move in the same direction. This is determined by whether the nanowire in a given post is tipped to the left or right of vertical relative to the field direction. As shown in Fig. 7, the post deflections all show hysteretic and approximately quadratic dependence at low fields. This reflects the hysteretic and linear low-field behavior of $\mu_\perp$ shown in Fig. 5. Displacements for nonmagnetic microposts are shown in Figs. 7(c) and 7(f) to indicate the accuracy of the measurement technique and registry error between frames. During the course of field modulation, nonmagnetic microposts had position fluctuations of ±0.05 μm, which we note as the lower detection limit with the image-threshold approach.

D. Calibration of magnetic micropost stiffness

The presence of an embedded nanowire in the upper portion of a magnetic micropost should increase the post's stiffness compared to that of nonmagnetic microposts. However, due to the flexibility in the lower portion of the micropost where there is no nanowire, a magnetic micropost still deflects in linear proportion to a force F_{tip} applied at its tip. A calculation using Castigliano's method [Eq. (2)] yields

$$\delta = \frac{64F_{\text{tip}}}{3\pi E_{\text{PDMS}} d^4}(L^3 - L_W^3), \tag{5}$$

again with the assumption that $E_{\text{Co}} \gg E_{\text{PDMS}}$. For the case $L_W = L/2$, this yields an effective spring constant $k_M = 3\pi E d^4/64(L^3 - L_w^3)$ that is 12.5% higher than for a nonmagnetic micropost [Eq. (1)].

To compare the microposts' spring constants, we used pulled-glass microneedles (World Precision Instruments, Sarasota, FL) to apply forces at the tips of individual

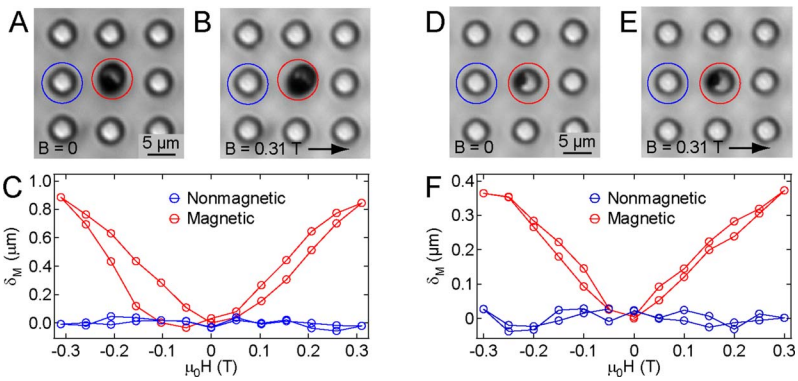

FIG. 7. (Color online) Characterization of magnetic micropost deflections. [(A) and (D)] Phase contrast image of magnetic microposts under zero field. [(B) and (E)] Applying a 0.31 T field causes deflection in the magnetic microposts. [(C) and (F)] Displacement δ_M vs applied field $\mu_0 H$ for magnetic and nonmagnetic microposts labeled in panels A and D.

microposts.[31] A microneedle was mounted on a probe positioner (DCM 220, Cascade Microtech, Beaverton, OR) and brought into contact with the tip of the micropost while observing under a microscope. The microneedle was then moved a measured distance with the probe positioner, which resulted in a force F_{tip} at the micropost that caused a displacement. We measured the displacement versus F_{tip} on six nonmagnetic and seven magnetic microposts, and compared the average spring constants $\bar{k}$ for each set. We found the ratio $\bar{k}_M/\bar{k}=1.05\pm0.16$ to be in reasonable agreement with our comparison of the simple models in Eqs. (1) and (5).

E. Mapping magnetic microposts

Prior to experiments with living cells on the arrays, the locations of the magnetic microposts on each array are mapped on a Nikon TE-2000 microscope with a 20× objective to provide a large field of view of the array. Phase contrast images of the microposts are taken at $\mathbf{B}=0$ and $\mathbf{B}=0.2$ T using the magnets on the sliding rails in the stage incubator. We locate magnetic microposts in the array with our image analysis program (Sec. IV C), which compares the centroid position of the microposts between images of 0 and 0.2 T fields to detect the magnetic deflections. A micropost with a deflection greater than 0.1 μm is identified as a magnetic micropost with sufficient force generation capability for cell stimulation experiments. We image the whole array by using its numbered grid to navigate over the array with the x-y stage of the microscope. In this manner, we can produce a complete map of the locations of each magnetic micropost and determine the external force transmitted to the cell from Eqs. (3) and (4). We find from these mappings that our fabrication method for the arrays yields an average density of one magnetic micropost for every 200 nonmagnetic microposts.

V. EXPERIMENTAL PROCEDURE

With our system, we can measure the prestimulation contractile activity in cells, apply external forces at individual adhesion sites, and then monitor the changes in cellular traction forces. To conduct these experiments, cells are first plated onto the functionalized micropost arrays and allowed to attach and spread across the tips of the microposts overnight in an incubator. The arrays are then transferred to a small rectangular culture dish and mounted on the magnetic stage incubator chamber (Fig. 4). A cell is selected for stimulation if it is attached to a magnetic micropost, as determined by cross referencing with the map for the array (Sec. IV E). Cells on the array that are not attached to magnetic microposts can be used as unstimulated controls. Phase contrast images of the cell and epifluorescence images of the microposts underneath and surrounding the cell are recorded with a 40× long working distance objective. Time courses that we have typically run to date consist of 10 min observation of a cell prior to applying the field, a stepwise field application, and then an additional 10 min of observation, with phase contrast and fluorescence image pairs recorded every 15 s. An example of such an image pair for a 3T3 fibroblast cell is shown in Fig. 8. The outer edge of the cell appears as a white

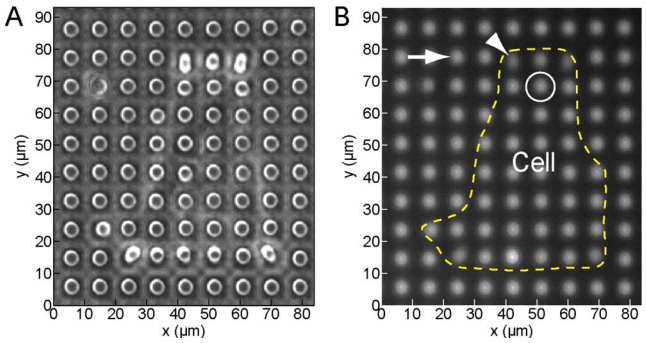

FIG. 8. (Color online) (A) Phase contrast image of the micropost array with a NIH 3T3 cell attached. (B) Fluorescent image of the same micropost array. The cell outline is traced from the corresponding phase contrast image. The arrow indicates a nonmagnetic micropost nearby the cell. The arrowhead indicates a nonmagnetic micropost to which the cell is attached. The circle indicates the location of the magnetic micropost.

diffuse line in the phase contrast image in Fig. 8(a), and this boundary is shown as a dashed line superimposed on the fluorescence image in Fig. 8(b). (We note that the cell boundary can be confirmed by observation of fluctuations in the membrane and cytoplasm from frame to frame as the cell probes its local environment.) Large deflections of some posts due to the cell's contractile forces can be clearly seen along the cell's top edge and at its bottom corners.

VI. IMAGE ANALYSIS AND FORCE DETERMINATION

The changes in a cell's traction force field in response to stimulation by a magnetic micropost are determined by measuring the microposts' deflections at each time point. These measurements are obtained from the fluorescence images using custom image analysis software (IGORPRO). For each micropost, the fluorescent pixel intensity data [Fig. 9(a)] are modeled to a two-dimensional Gaussian profile [Fig. 9(b)] determined by a least-squares fit to the spatial image data. The Gaussian function used is given by

$$\Phi(x,y)=z_0+A\exp\left\{-\frac{1}{2(1-\sigma^2)}\left[\left(\frac{x-x_0}{x_w}\right)^2+\left(\frac{y-y_0}{y_w}\right)^2-\frac{2\sigma(x-x_0)(y-y_0)}{x_w y_w}\right]\right\}, \tag{6}$$

where z_0 is the background intensity, A is the intensity amplitude, σ is the cross correlation (with limits of $-1\leqslant\sigma\leqslant1$), x_w and y_w are the Gaussian widths, and y_0 and x_0 give the position of the center of the top of the micropost. Equation (6) closely matches the intensity profile of the data, as shown by the line cuts in Figs. 9(c) and 9(d) which compare the fluorescence data to the fitted Gaussian function along the x- and y-centerlines in Fig. 9(a). We find the uncertainty in the least-squares fit for determining the centers of microposts in the array to be less than 8.4 nm at a given time point, but there are larger fluctuations during the 20 min of observation due to image registration.

A set of microposts not attached to the cell but bordering it (free posts) is used for frame-to-frame registration and as reference marks for determining the undeflected positions of the microposts underneath the cell. An example of this is the

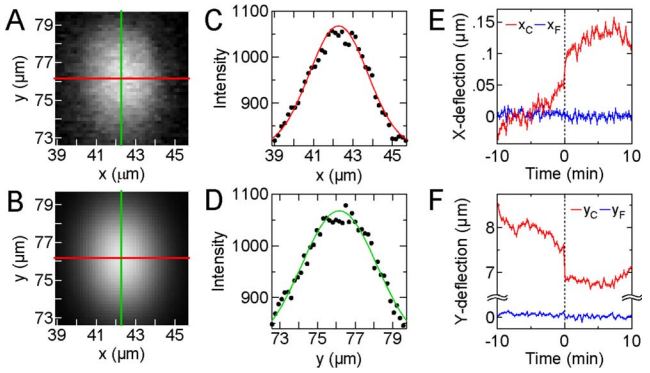

FIG. 9. (Color online) Image analysis for measuring the deflections of the microposts. (A) Image of a micropost [arrowhead in Fig. 8(b)] with an applied traction force by the cell. The center of the micropost is identified with an x-center line (red) and y-center line (green). (B) Two-dimensional Gaussian curve fit for the image data in panel B. (C) Gaussian fit data (red line) compared with image data (black dots) along the x-center line. (D) Gaussian fit data (green line) compared with image data (black dots) along the y-center line. [(E) and (F)] Plots of calculated x- and y-deflections vs time for the post in panel A (red, subscript "C") and a free post (blue, subscript "F") identified in Fig. 8(b) with an arrow. The field is turned on at $t=0$ and a force $F_{\mathrm{mag}}=3.33$ nN is applied in the positive y-direction at the magnetic post. Error bars indicate uncertainty in image analysis.

micropost designated with an arrow in Fig. 8(b). Our image analysis software conducts a linear regression using a least-squares line fit through the center positions of the free posts in a given row or column. The intersections of these lines define the undeflected positions of the microposts. To ensure an accurate determination of these lines, we image the cell so that there are three or more free posts to either side of the cell in a given row or column (Fig. 8 has been cropped to highlight the cell). Displacements are determined from the difference between the measured center of the top of a micropost (x_0 and y_0) determined from the two-dimensional Gaussian fit and its undeflected position. With this approach, free posts have a displacement error that on average is less than 80 ± 50 nm due to irregularities in the array that affect the least-squares line fit. Representative image analysis results for the deflected positions of microposts during the course of the experiment are shown in Figs. 9(f) and 9(g). Here, we plot the x- and y-deflections over time for the two posts indicated in Fig. 8(b), a "cell post" that is in contact with the cell [arrowhead in Fig. 8(b)], and a "free post" that is not in contact with the cell [arrow in Fig. 8(b)]. The post in contact with the cell shows a slight x-deflection (x_C) and a large y-deflection (y_C) due to the cell's traction force. During the course of the measurement, the deflection of the free post (x_F and y_F) remains negligible. When the 0.2 T field is applied ($t=0$), a force ($F_{\mathrm{mag}}=3.33$ nN) is applied to the cell in the positive y-direction via the magnetic post indicated by a white circle in Fig. 8(b). At the next time point ($t=15$ s), an abrupt change in position is detected at the cell post ($\Delta x_C = 34$ nm, $\Delta y_C = -133$ nm), indicating a decrease in traction force ($\Delta F_C = -4.4$ nN). The change in position of the free post when the field is applied ($\Delta x_C = -7$ nm, $\Delta y_C = -19$ nm) is indistinguishable from the fluctuations due to measurement uncertainty observed over the whole time course. This example shows how the traction forces at each micropost can be accurately tracked over time and how the free posts serve as reference points for image analysis.

To demonstrate the type of experiments possible with the magnetic micropost system, Fig. 10(a) shows all of the traction force vectors for the cell in Fig. 8 before applying the magnetic field ($t=-0.15$ min). These force vectors were obtained from the deflection data using the spring constant of 32 nN/μm. Upon application of the field, there is an abrupt decrease in the traction forces at multiple cell posts, which are labeled in Fig. 10(b) ($t=+0.35$ min). Figure 10(c) shows the traction forces of all cell posts (pink), the cell posts labeled 1–5 in Fig. 10(b) (red), and the magnetic post (black), which is labeled "m" in Fig. 10(b). The magnetic post exhibited a change in force after the field is applied (0.3 nN); however, this change is smaller than what was measured before plating cells (3.3 nN), indicating that the cell provides a counterbalancing force against the magnetic micropost which reduced the deflection. For $t<0$, the cell posts have slow changes in traction forces, demonstrating that the cell is maintaining a steady level of baseline contractility. However, force application causes traction force losses at the cell posts labeled 1–5 along the cell's perimeter. Note that several of these are at locations remote from the point of stimulation. Detection of such nonlocal cellular responses illustrates the unique capability of the magnetic micropost system to measure spatiotemporal phenomena of the cytoskeleton in response to force stimulation. For example, it should be possible to probe polarized cells that have heterogeneous localities in their cytoskeleton that may influence the nonlocal response and may affect cellular function such as mechanically directed migration, also know as durotaxis.[39]

VII. SUMMARY

The system presented here employs embedded magnetic nanowires and flexible microposts to apply and measure traction forces in biological cells. The large range of forces that can be applied is due to the high magnetic moments $\boldsymbol{\mu}$ of the embedded cobalt nanowires. A key feature of this approach is its capability to conduct force stimulation and measurement in a simultaneous fashion. The magnetic microposts

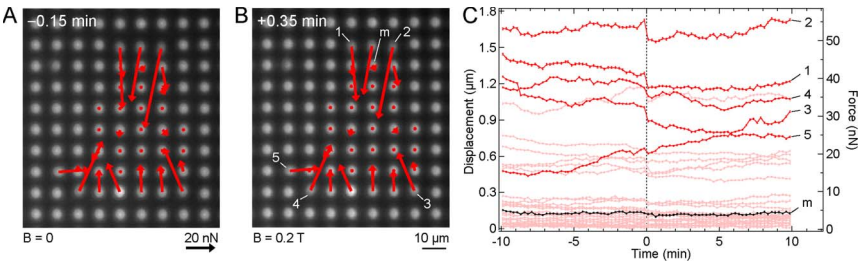

FIG. 10. (Color online) Live-cell force microscopy results. [(A) and (B)] Red arrows show traction forces before ($t=-0.15$ min) and after ($t=+0.35$ min) application of external force calculated from fluorescent image of the array. Force stimulation at $t=0$ leads to nonlocal changes in the contractility of the cell. (C) Displacement and traction forces vs time for the cell posts (pink), a subset of cell posts labeled in panel B (red), and the magnetic micropost (black).

have similar bending stiffness as the nonmagnetic microposts and can function as sensors as well as actuators during the course of the experiments, depending on the state of the applied magnetic field. The bed of nonmagnetic microposts underneath the cell provides a spatial readout of the traction forces throughout the cell.

We have only used the system to date for short-duration (20 min) experiments, but longer observation periods are possible. We have on occasion extended the observations to as long as 1 h, and the stability of the live-cell incubator controller is sufficient to enable runs of several hours. Faster image acquisition rates than the one frame per 15 seconds we have illustrated here are also feasible, but ultimately may be limited by the exposure time for the fluorescence images of the microposts (1 s in our current implementation) and the time needed to move the magnets and possibly refocus the microscope when changing the field with the sliding rail mechanism.

We have transmitted mechanical signals to FAs up to 45 nN, which is competitive with the current upper limit of other force-probing systems. Larger forces should be possible with higher fields, as the Co nanowires are far from magnetic saturation at the fields we have employed. Such fields should be readily achievable with more sophisticated magnet designs than used here. Nonetheless, our system closely matches the range of traction forces generated by cells, and so it can probe biologically relevant force scales of cells. By using ac magnetic fields, it should also be possible to modulate the external force, and we have verified that the magnetic microposts can be driven at frequencies up to 5 Hz without significant damping effects due to the viscoelastic properties of PDMS.[40]

In summary, the magnetic micropost array system presented here enables explorations into the interrelationship between traction forces and external forces in cells, and should facilitate deeper probes into the mechanobiology of cellular systems.

ACKNOWLEDGMENTS

This work was supported in part by grants from the National Heart, Lung, and Blood Institute (HL080054 and HL73305), the National Institute of Biomedical Imaging and Bioengineering (EB00262), the National Institute of General Medical Sciences (GM74048), the Army Research Office Multidisciplinary University Research Initiative, the Materials Research Science and Engineering Center of Johns Hopkins University (DMR-0520491), and the Nano/Bio Interface Center of the University of Pennsylvania (DMR-0425780). N.J.S. acknowledges financial support by the Hartwell Foundation and the Ruth L. Kirschstein National Research Service Award.

[1] D. E. Ingber, Ann. Med. **35**, 564 (2003).
[2] B. Geiger, A. Bershadsky, R. Pankov, and K. M. Yamada, Nat. Rev. Mol. Cell Biol. **2**, 793 (2001).
[3] F. J. Alenghat and D. E. Ingber, Science STKE **2002**, PE6 (2002).
[4] D. Choquet, D. P. Felsenfeld, and M. P. Sheetz, Cell **88**, 39 (1997).
[5] C. G. Galbraith, K. M. Yamada, and M. P. Sheetz, J. Cell Biol. **159**, 695 (2002).
[6] Y. Wang, E. L. Botvinick, Y. Zhao, M. W. Berns, S. Usami, R. Y. Tsien, and S. Chien, Nature (London) **434**, 1040 (2005).
[7] N. Wang, J. P. Butler, and D. E. Ingber, Science **260**, 1124 (1993).
[8] M. Glogauer, P. Arora, D. Chou, P. A. Janmey, G. P. Downey, and C. A. McCulloch, J. Biol. Chem. **273**, 1689 (1998).
[9] B. D. Matthews, D. R. Overby, R. Mannix, and D. E. Ingber, J. Cell. Sci. **119**, 508 (2006).
[10] D. Riveline, E. Zamir, N. Q. Balaban, U. S. Schwarz, T. Ishizaki, S. Narumiya, Z. Kam, B. Geiger, and A. D. Bershadsky, J. Cell Biol. **153**, 1175 (2001).
[11] I. Kaverina, O. Krylyshkina, K. Beningo, K. Anderson, Y. L. Wang, and J. V. Small, J. Cell. Sci. **115**, 2283 (2002).
[12] G. T. Charras and M. A. Horton, Biophys. J. **82**, 2970 (2002).
[13] H. Huang, R. D. Kamm, and R. T. Lee, Am. J. Physiol.: Cell Physiol. **287**, C1 (2004).
[14] V. Vogel and M. Sheetz, Nat. Rev. Mol. Cell Biol. **7**, 265 (2006).
[15] A. Bershadsky, M. Kozlov, and B. Geiger, Curr. Opin. Cell Biol. **18**, 472 (2006).
[16] S. Hu, J. Chen, B. Fabry, Y. Numaguchi, A. Gouldstone, D. E. Ingber, J. J. Fredberg, J. P. Butler, and N. Wang, Am. J. Physiol.: Cell Physiol. **285**, C1082 (2003).
[17] R. Blumenfeld, Biophys. J. **91**, 1970 (2006).
[18] D. E. Discher, P. Janmey, and Y. L. Wang, Science **310**, 1139 (2005).
[19] G. Giannone and M. P. Sheetz, Trends Cell Biol. **16**, 213 (2006).
[20] K. A. Beningo and Y.-L. Wang, Trends Cell Biol. **12**, 79 (2002).
[21] N. J. Sniadecki, R. A. Desai, S. A. Ruiz, and C. S. Chen, Ann. Biomed. Eng. **34**, 59 (2006).
[22] A. K. Harris, P. Wild, and D. Stopak, Science **208**, 177 (1980).
[23] J. Lee, M. Leonard, T. Oliver, A. Ishihara, and K. Jacobson, J. Cell Biol. **127**, 1957 (1994).
[24] M. Dembo, T. Oliver, A. Ishihara, and K. Jacobson, Biophys. J. **70**, 2008 (1996).
[25] N. Q. Balaban, U. S. Schwarz, D. Riveline, P. Goichberg, G. Tzur, I. Sabanay, D. Mahalu, S. Safran, A. Bershadsky, L. Addadi, and B. Geiger, Nat. Cell Biol. **3**, 466 (2001).
[26] J. L. Tan, J. Tien, D. M. Pirone, D. S. Gray, K. Bhadriraju, and C. S. Chen, Proc. Natl. Acad. Sci. U.S.A. **100**, 1484 (2003).
[27] O. du Roure, A. Saez, A. Buguin, R. H. Austin, P. Chavrier, P. Siberzan, and B. Ladoux, Proc. Natl. Acad. Sci. U.S.A. **102**, 2390 (2005).
[28] N. J. Sniadecki, A. Anguelouch, M. T. Yang, C. M. Lamb, Z. Liu, S. B. Kirschner, Y. Liu, D. H. Reich, and C. S. Chen, Proc. Natl. Acad. Sci. U.S.A. **104**, 14553 (2007).
[29] C. A. Lemmon, N. J. Sniadecki, S. A. Ruiz, J. L. Tan, L. H. Romer, and C. S. Chen, Mech. Chem. Biosyst. **2**, 1 (2005).
[30] F. P. Beer and E. R. Johnston, *Mechanics of Materials* (McGraw-Hill, New York, 1981).
[31] N. J. Sniadecki and C. S. Chen, Methods Cell Biol. **83**, 313 (2007).
[32] Y. N. Xia and G. M. Whitesides, Angew. Chem. **37**, 551 (1998).
[33] J. L. Tan, W. Liu, C. M. Nelson, S. Raghavan, and C. S. Chen, Tissue Eng. **10**, 865 (2004).
[34] A. Encinas-Oropesa, M. Demand, L. Piraux, I. Huynen, and U. Ebels, Phys. Rev. B **63**, 104415 (2001).
[35] C. Z. Li and J. C. Lodder, J. Magn. Magn. Mater. **88**, 236 (1990).
[36] A. H. Morrish, *The Physical Principles of Magnetism* (Wiley, New York, 1965).
[37] Y. Henry, K. Ounadjela, L. Piraux, S. Dubois, J. M. George, and J. L. Duvail, Eur. Phys. J. B **20**, 35 (2001).
[38] A. Hultgren, M. Tanase, C. S. Chen, G. J. Meyer, and D. H. Reich, J. Appl. Phys. **93**, 7554 (2003).
[39] C. M. Lo, H. B. Wang, M. Dembo, and Y. L. Wang, Biophys. J. **79**, 144 (2000).
[40] C. M. Lamb, Y. Liu, N. J. Sniadecki, C. S. Chen, and D. H. Reich (unpublished).